Anomalous precipitation signatures of the Arctic Oscillation in the time-variable gravity field by GRACE

Koji Matsuo and Kosuke Heki

Department of Natural History Sciences, Hokkaido University, N10 W8, *Kita-ku, Sapporo, Hokkaido* 060–0810, *Japan.*
E-mail: kouji-matsuo@mail.sci.hokudai.ac.jp

SUMMARY

The Arctic Oscillation (AO) controls winter climates in the Northern Hemisphere to a large extent. Positive AO brings lower/higher surface temperature and higher/lower precipitation in high/middle latitude regions, and negative AO reverses the situation. In this study, we investigate signals of anomalous precipitations caused by AO using the data of the Gravity Recovery and Climate Experiment (GRACE) satellites. Wintertime mass deviations inferred from GRACE in the high and middle (boundary ∼55N) latitude regions in Eurasia showed highly positive and negative correlations with the AO indices. This possibly reflects the northward and southward shift of the centre of winter precipitation during the positive and negative phases of AO, respectively. Wintertime mass deviations also showed positive and negative correlations with the AO indices in the northern and southern parts of Greenland, respectively, but the boundary was further to the north, say ∼75N. AO redistributes the water mass as much as ∼1000 Gt between high and middle latitude regions in the Northern Hemisphere. Such mass redistribution causes significant surface deformation by loading large enough to be observed by Global Positioning System. This also causes the shift of the Earth's rotation axis especially towards the Greenwich Meridian large enough to be detected with space geodetic techniques. AO signatures are also derived from the empirical orthogonal function (EOF) analysis, as the first leading mode of GRACE data after excluding seasonal, linear and quadratic components. The EOF analysis also demonstrates that though AO is a main contributor to bring anomalous winter precipitation in the Northern Hemisphere as a whole, in North America, however, influence of the El Niño and Southern Oscillation on the winter precipitation anomaly is larger than AO.

Key words: Satellite geodesy; Transient deformation; Time variable gravity; Earth rotation variations; Global change from geodesy; Arctic region.

GJI Gravity, geodesy and tides

1 INTRODUCTION

Arctic Oscillation (AO) is a see-saw-like fluctuation in the sea level pressure (SLP) between polar and middle latitude regions of the Northern Hemisphere (NH), and its index characterizes the dominant pattern of atmospheric circulation in NH (Thompson & Wallace 1998). AO resembles to the North Atlantic Oscillation (NAO), a see-saw of SLP between the Icelandic low and the Azores high (Walker & Bliss 1932), but AO represents the variability in the atmospheric circulation of the whole NH (Wallace 2000). Their indices are known to have high temporal correlation. There are some debates as to their differences (e.g. Ambaum *et al.* 2001), but here we consider NAO a part of AO.

AO exerts strong influences on wintertime climate in NH (Thompson & Wallace 2000). The scale and phase of AO is represented by the AO index (AOI) derived as the first leading mode of empirical orthogonal function (EOF) of monthly mean SLP anomaly

field north of 20N. AOI becomes positive when SLP around the North Pole is lower than the average. Positive AO brings the retention of arctic cold surge and enhancement of polar front jet (PFJ), the northern stream of the westerly jet, causing low temperature and high precipitation (mainly snowfall) in the high latitude regions (Hurrell 1995; Thompson & Wallace 2001). The opposite occurs in the middle latitude regions. On the other hand, AOI becomes negative when SLP around the North Pole gets higher than the average. Negative AO is characterized by the southward advection of arctic cold wave and southward shift of PFJ, and it causes low temperature and high precipitation (rainfall and snowfall) in the middle latitude regions. The opposite occurs in the high latitude regions.

Fig. 1 shows the time-series of AOI between 2002 April and 2011 March. In the NH winter of 2009–2010, the record-breaking strong negative AO occurred, and brought about anomalous precipitation and temperature in various regions in middle latitude regions (Cohen *et al.* 2010; L'Heureux *et al.* 2010; Wang *et al.* 2010).
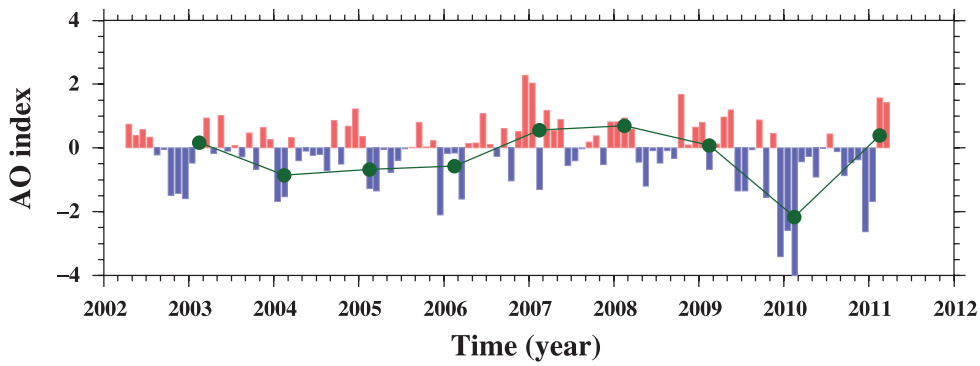
Figure 1. Time-series of the monthly AO index from National Oceanic and Atmospheric Administration (http://www.cpc.ncep.noaa.gov/products/precip/CWlink/daily_ao_index/ao.shtml). Red and blue bars show positive and negative phases of AO, respectively. The green curve shows the time series of the three month (JFM) averages of AO indices in NH winters.

Precipitation changes the Earth's gravity fields as it redistributes water on land and ocean. Such mass redistribution can be detected and measured by the Gravity Recovery and Climate Experiment (GRACE) satellite system, composed of twin satellites launched in 2002. The two satellites, separated by $\sim$220 km, are in the same polar circular orbit at an altitude of $\sim$500 km, and the change of the intersatellite distances are measured precisely. The time-variable gravity fields of the Earth are inverted from the changes of such distances. The gravity measured by GRACE is accurate to several μGal, and has spatial and temporal resolutions of $\sim$300 km and $\sim$1 month, respectively (Wahr *et al.* 1998).

Up to now, GRACE results have been utilized for various disciplines of Earth sciences, such as hydrology (e.g. Tapley *et al.* 2004; Morishita & Heki 2008), glaciology (e.g. Tamisiea *et al.* 2005; Matsuo & Heki 2010), physical oceanography (e.g. Chambers *et al.* 2004), seismology (e.g. Han *et al.* 2006; Matsuo & Heki 2011) and geodynamics (e.g. Tamisiea *et al.* 2007). The advantage of satellite gravimetry is the direct and quantitative measurement of mass changes, especially in regions where *in situ* observations are limited, for example, polar and high mountain regions. In this paper, we discuss wintertime precipitation anomalies caused by AO in NH by analysing the time-variable gravity data from GRACE. To further validate the GRACE results, we also analysed the changes in terrestrial water (including snow) storage given by the Global Land Data Assimilation System (GLDAS) Noah model (Rodell *et al.* 2004).

2 DATA AND METHOD

We used the GRACE data (Level 2, Release 4) from the Center for Space Research (CSR), University of Texas, consisting of 103 monthly data sets from 2002 April to 2011 March. This time span covers nine winters in NH. A monthly GRACE data set includes a set of the coefficients of spherical harmonics (Stokes' coefficient) C_{nm} and S_{nm} with degree n and order m complete to 60. We replaced the coefficients indicating the Earth's oblateness (C_{20}) with those from Satellite Laser Ranging (Cheng & Tapley 2004) because of their poor accuracy. We used the degree-1 components (C_{10}, C_{11} and S_{11}), which reflect the geocentre motion, estimated by combining GRACE and ocean model (Swenson *et al.* 2008) because GRACE alone cannot measure them. We also applied the fan filter with averaging radius of 400 km to reduce short wavelength noises (Zhang *et al.* 2009), together with the decorrelation filter using polynomials of degree 5 for coefficients with orders 6 or higher to alleviate longitudinal stripes (Swenson & Wahr 2006).

To interpret gravity changes in terms of surface mass variations, we need to calculate equivalent water thickness (EWT) σ using the relationship (Wahr *et al.* 1998)

$$\Delta\sigma(\theta, \phi) = \frac{R\rho_{\text{ave}}}{3} \sum_{n=2}^{\infty} \sum_{m=0}^{n} \frac{2n+1}{1+k_n}$$
$$\times (\Delta C_{nm} \cos m\phi + \Delta S_{nm} \sin m\phi) P_{nm}(\sin\theta),$$

where R is the equatorial radius, ρ_{ave} is the mean density of the Earth, and the load Love numbers k_n is to account for the Earth's elastic yielding effect under the mass load in question. $P_{nm}(\sin\theta)$ is the nth degree and mth order fully-normalized Legendre function and Δ indicates the deviation from the reference value. We assumed that the GRACE gravity changes reflect those of the surface load, and converted them into EWT. Chao (2005) showed that the inverse solution is unique in this case.

Temporal variations of EWT contain mass changes of various origins. Such changes usually include strong seasonal (annual and semi-annual) and linear components. Seasonal changes mainly come from the variations in soil moisture and snowpack (Frappart *et al.* 2006; Schmidt *et al.* 2008). Linear changes reflect secular mass movements, such as glacial isostatic adjustment in North America and northern Europe (Tamisiea *et al.* 2007; Steffen *et al.* 2009), and ice melting in continental ice sheets (e.g. Velicogna & Wahr 2006a,b) and mountains glaciers (e.g. Chen *et al.* 2006).

In addition to these components, quadratic changes became evident as the GRACE data accumulated. Ogawa *et al.* (2011) showed that quadratic terms seen in the GRACE data are often explained by interannual changes in precipitation. Gardner *et al.* (2011) also showed that quadratic gravity changes are significant in the Canadian Arctic Archipelago, and suggested that it reflects accelerating melting of mountain glaciers and ice caps there over the last several years. To isolate AO signals from these mass changes, we remove seasonal, linear and quadratic components from the EWT time-series by least-squares method. Here, we refer to the residual as equivalent water thickness deviation (EWD). Then we calculate averages of the three winter months (JFM; January, February and March) to discuss mass changes in NH winters.

In addition to GRACE, we have also used monthly solutions of the changes in terrestrial water storage by the GLDAS Noah model (Rodell *et al.* 2004). GLDAS provides soil moisture, canopy and snow data at 1×1 degree grid points, except for Antarctica where hydrological models are not established and meteorological data are unavailable. GLDAS contains the values in Greenland, but their

accuracy is dubitable because of the same reason as Antarctica. So we did not use the GLDAS model in the Greenland area. To compare GLDAS with GRACE, we applied the same spatial filters (fan filter and destriping filter) for the GLDAS models and removed seasonal, linear and quadratic components by the least-squares method. Then we also calculated their averages of months JFM.

3 RESULTS

3.1 GRACE and GLDAS

Following the analysis methods in the previous section, we plot the EWD distributions in NH to the north of 25N in the winters from 2003 ('2003 winter' means the NH winter encompassing the 2002–2003 boundary) to 2011 in Fig. 2 (GRACE) and Fig. 3 (GLDAS). Their spatial patterns roughly agree with each other, but small differences in magnitudes remain.

Syed *et al.* (2008) suggested that such difference in magnitudes may reflect model deficiencies in GLDAS, such as inadequate snow models in high mountain ranges and polar regions, missing surface and/or groundwater components, and so on. The difference might also reflect errors in GRACE data processing, aliasing or instrumental noises. Moreover, GRACE data includes mass change signals from semi-closed ocean basins (or large lakes) such as the Mediterranean Sea (Fenoglio-Marc *et al.* 2006), Black Sea, Caspian Sea and Red Sea, but GLDAS does not include them. Leakage from such signals might have enhanced the signals of terrestrial mass changes. From these reasons, the magnitudes of EWT or EWD in GLDAS are apt to become smaller than those in GRACE.

The largest positive (AOI = +0.8) and negative (AOI = −2.4) AO in the studied period occurred in the winters of 2008 and 2010,

respectively. The EWD distributions in these two winters show characteristic spatial patterns (Figs 2 and 3). The polarity of EWD reverses across the latitude 55N in Eurasia continent and North America and 75N in Greenland. It also reverses temporally between these two winters. Especially, the winter of 2010 witnessed the largest negative AO in the last 60-yr record, causing record-breaking precipitations in many parts of the middle latitude regions of NH, such as the southern North America (Seager *et al.* 2010) and southern Europe (Ball 2011).

3.2 Microscopic view of the correlation between the GRACE/GLDAS and AO

We plot the time-series of monthly and wintertime EWD obtained by GRACE and GLDAS at two points, that is the Western Siberia and Tien-Shan Mountain Range, representing the high and the middle latitude regions in Eurasia in Figs 4(a) and (b), respectively. Fig. 4 also shows the time-series of the wintertime AOI. Wintertime EWDs in the Western Siberia, inferred from GRACE and GLDAS, showed positive/negative deviations during periods of positive/negative AO indices. On the other hands, those in the Tien-Shan Mountain Range showed the opposite; negative/positive deviation occurred during AO of positive/negative indices. The wintertime EWD and AOI showed large positive correlation in Western Siberia, that is +0.95 (GRACE) and +0.84 (GLDAS). These positive correlations mean that the positive/negative AO increased/decreased the terrestrial water storages in these regions. By contrast, they showed significant negative correlation in the Tien-Shan Mountain Range, that is −0.68 (GRACE) and −0.70 (GLDAS). These negative correlations imply that the positive/negative AO decreased/increased the terrestrial water storages there.
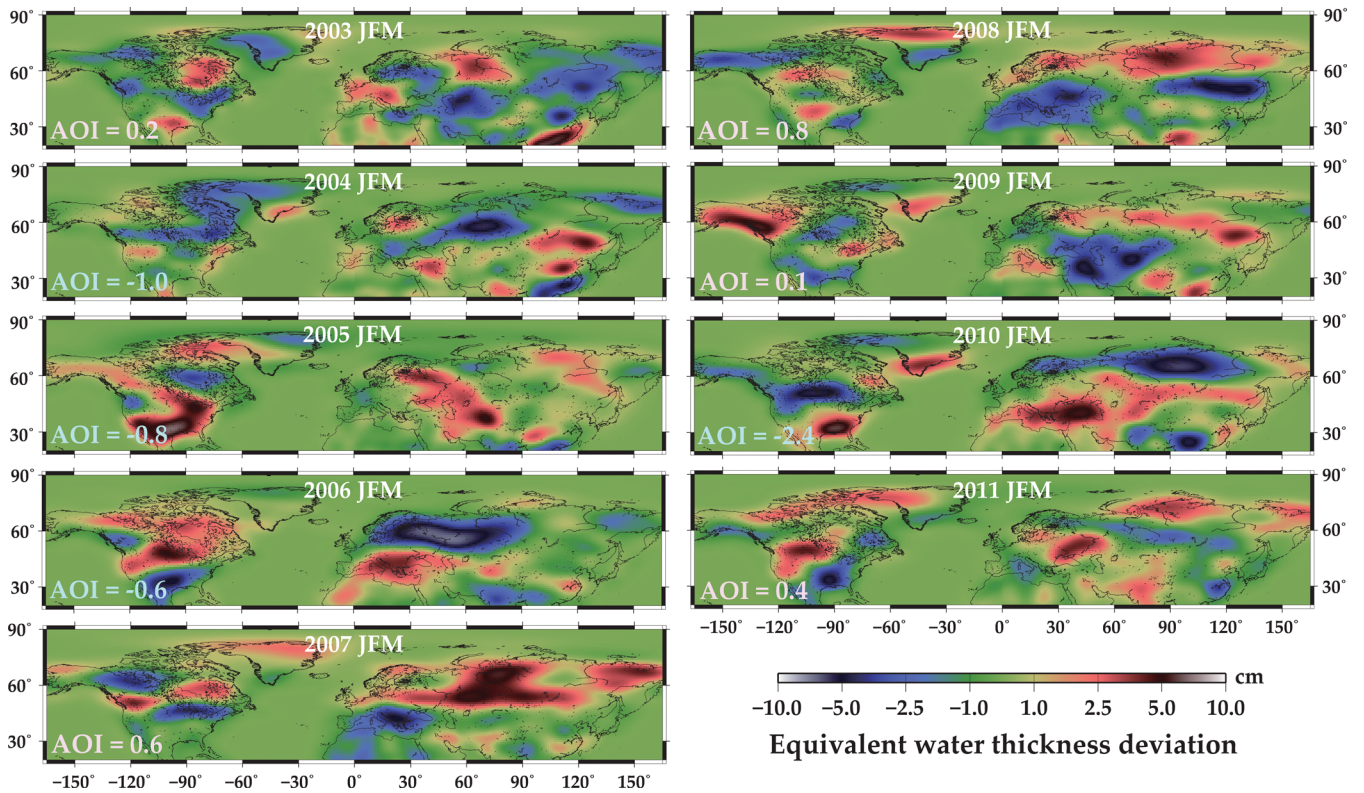

Figure 2. NH maps of wintertime (JFM) equivalent water thickness deviations observed by GRACE. In the lower left corners of the maps are shown AOI corresponding to the green curve in Fig. 1.
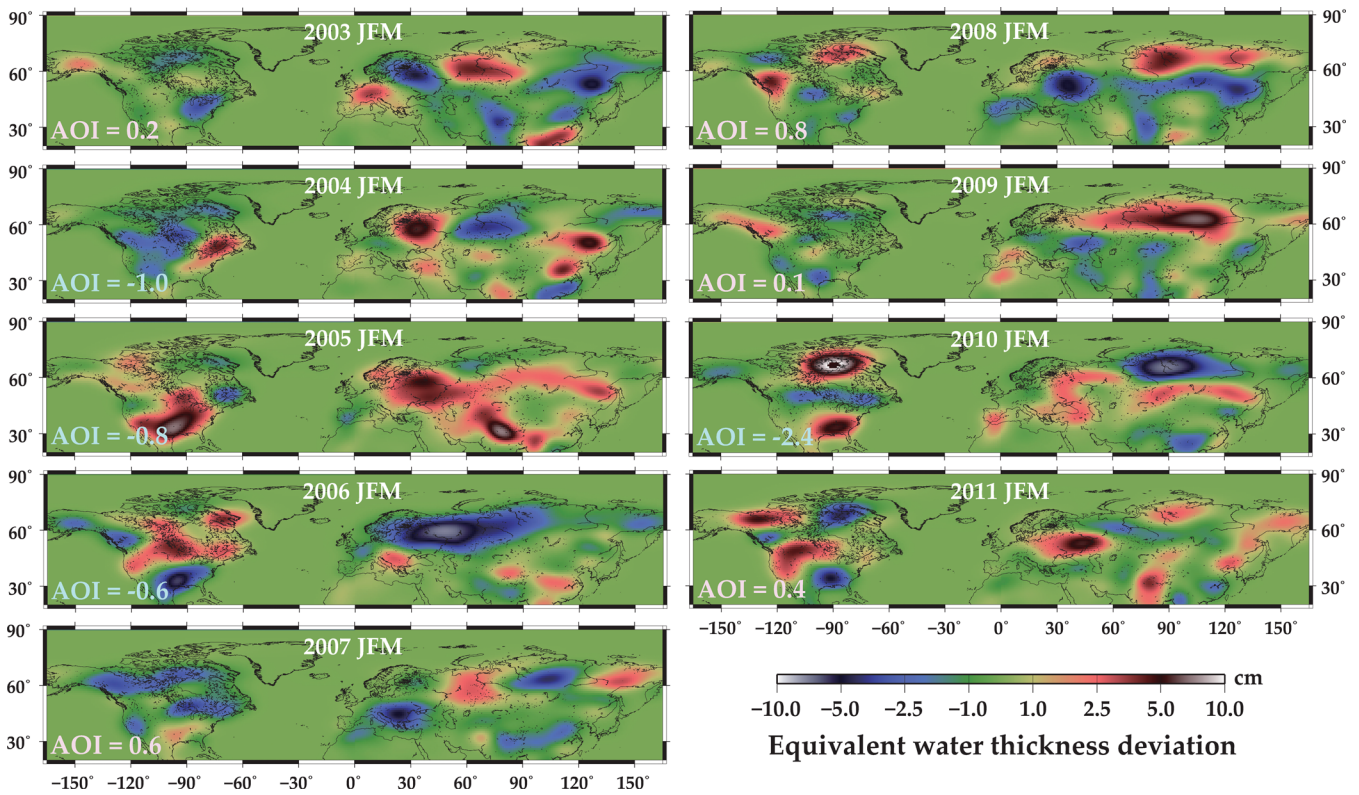
Figure 3. NH maps of wintertime (JFM) equivalent water thickness deviation from the GLDAS models. The same spatial filters as GRACE have been applied. We excluded Greenland (values are fixed to zero there) because of relatively poor reliability there (see text).
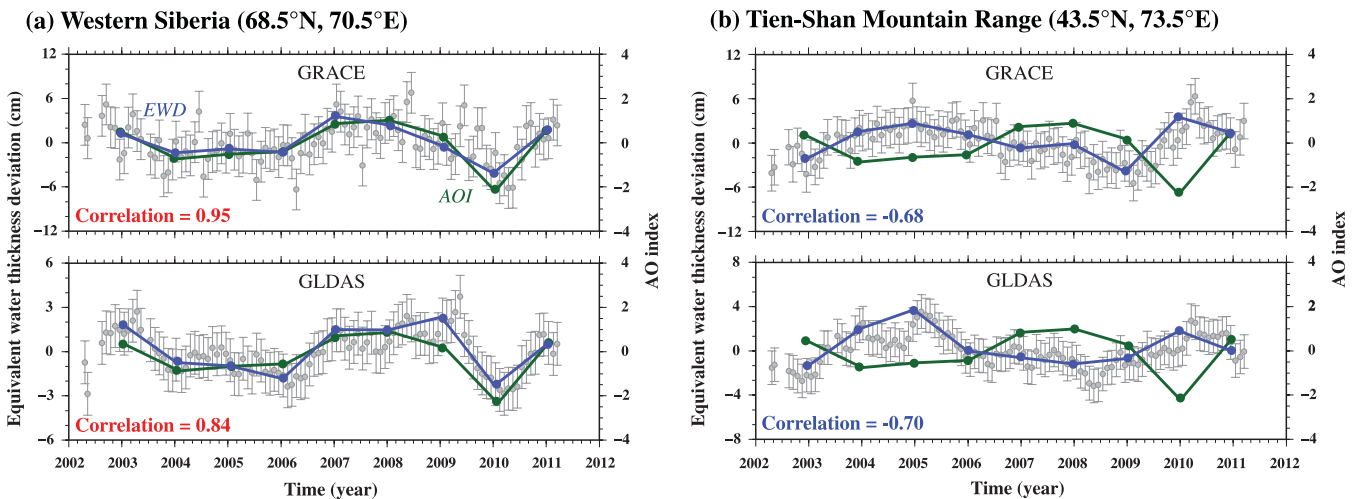

Figure 4. Time-series of EWD at points in (a) the Western Siberia (68.5N, 70.5E) and (b) the Tien-Shan Mountain Range (43.5N, 73.5N). The top and the bottom panels are derived from GRACE and GLDAS, respectively. Grey dots are monthly values of EWD. Error bars show one-sigma formal errors inferred *a posteriori* by bringing the chi-square of the post-fit residual to unity. Blue curves are the three-month (JFM) averages of the EWDs. Green curves show winter AOI (Fig. 1, green curve). The correlation coefficients between wintertime EWDs and AOI are given in the lower left corners (red and blue characters show positive and negative correlations, respectively).

Matsuo & Heki (2010) suggested that glacial mass in Asian high mountains (HM Asia) surrounding the Tibetan Plateau shows significant decrease using the GRACE data 2002–2009. They also reported that glacial mass losses are fairly variable in time and space, especially in the glaciers fed by westerly winds from November to April such as those in the Karakorum, Pamir and Tien-Shan regions. AO is known to influence the strength and trajectory of the westerly wind (Thompson & Wallace 2000). This study suggests that climatic

fluctuations controlled by AO played a key role in the glacial mass changes in these regions.

3.3 Macroscopic view of the correlation

Next we computed correlation coefficients between the wintertime EWD and AOI at each grid points in NH, and show their distribution
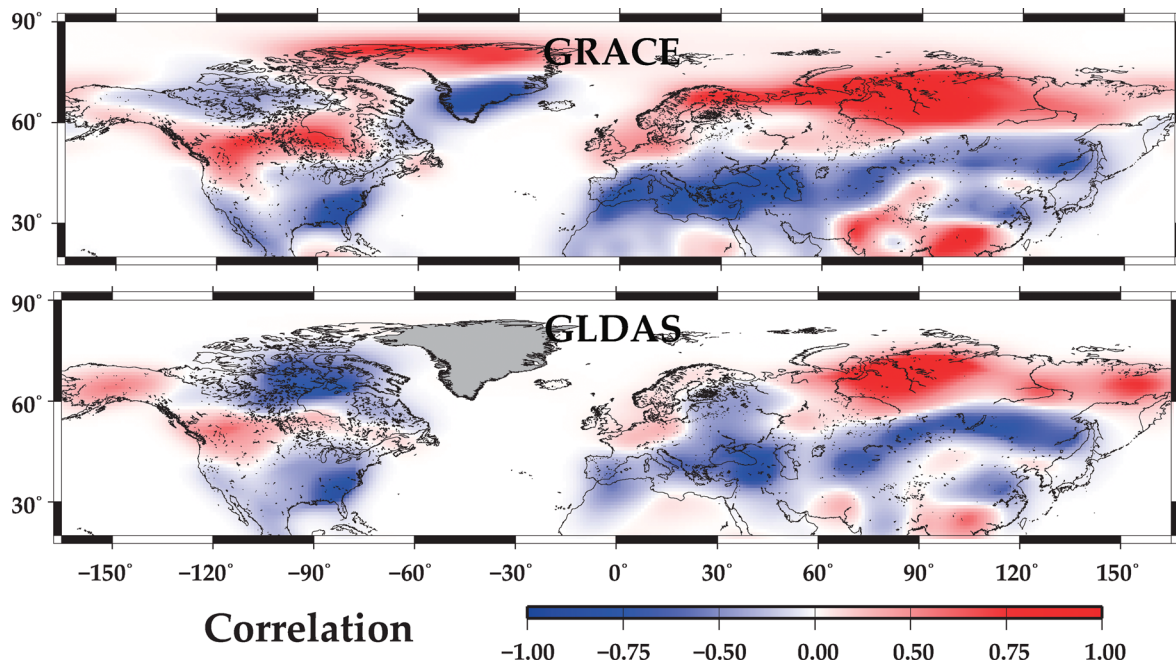
Figure 5. Distribution of the correlation coefficients between wintertime EWDs and AO indices for GRACE (top) and GLDAS (bottom) at grid points in NH. We excluded Greenland in the GLDAS models (pasted in grey). The boundary between the positive and negative correlations lies ∼55N in Eurasia and North America for both GRACE and GLDAS, and ∼75N in Greenland for GRACE.

in Fig. 5. We can find that high latitude region is dominated by positive correlation, and middle latitude region is dominated by negative correlation. This means that wintertime precipitation increases in the high latitude region during positive AO. On the other hand, such an increase in the middle latitude region occurs during negative AO. This agrees with climatological studies that a negative AO makes the southern and the northern Europe wetter and drier, respectively (Quadrelli *et al.* 2001; Hurrell *et al.* 2003). It appears that the boundary of the polarity change lies ∼55N in Eurasia and North America, and ∼75N in Greenland.

Though the North American continent shows similar distribution of the correlation to Eurasia, climatic situation is somewhat more complex there. Wintertime precipitations in North America are highly influenced by El Niño and Southern Oscillation (ENSO) episodes as well as AO. According to Ropelewski & Halpert (1987), El Niño/La Niña episodes tend to cause more/less precipitation in southeastern United States and less/more precipitation in northwestern North America, respectively. Thus, we need more sophisticated numerical studies there to separate contributions from AO and ENSO. We discuss the influences of ENSO and other climatic modes on the mass changes in NH in the chapter 4.

AO also exerts strong influence on the total amount of precipitation and EWD changes in NH, especially in Eurasia. Here we integrate EWD in Eurasia from GRACE and GLADS over high (55N to 90N, −15E to 165E) and middle (25N to 55N, −15E to 165E) latitude regions, and show their time-series in the top two panels in Figs 6(a) and (b). The time-series of the sum of and the difference between these two regions are shown in the bottom two panels of the same figure. Total masses in the high latitude region are positively correlated with AO, that is +0.69 for GRACE and +0.42 for GLDAS. On the other hands, those in the middle latitude region are negatively correlated with AO, that is −0.81 for GRACE and −0.61 for GLDAS. In short, stronger positive/negative AOI brings more precipitations in the high/middle latitude regions, respectively.

The sum of mass deviations in the high and middle latitude regions does not show notable correlation with AO. They are only weakly correlated negatively, that is −0.35 for GRACE and −0.30 for GLDAS. In contrast, the difference between the high and middle latitude regions shows strong correlations with AO, that is +0.89 for GRACE and +0.76 for GLDAS. This suggests that the centre of precipitation anomalies moves between high and middle latitude regions in response to the polarity of AO. The water mass that moves between these two latitudinal bands amounts up to ∼1000 Gt in the studies period. However, the total mass over the entire region changes only a little. The slight increase of the total mass during periods of negative AO may partly reflect the difference in land area between the middle and high latitude regions (the former has continental area twice as large as the latter, and so its hydrological capacity is also larger).

3.4 Surface deformation by AO

Mass redistribution by AO leaves non-gravity signatures in the solid Earth detectable with other geodetic techniques. Anomalous precipitation by AO brings surface loads and causes crustal deformation, which can be directly measured with Global Positioning System (GPS). We can also infer such deformation from the GRACE data through elastic loading theory on the spherical Earth using the load Love numbers (Farrell 1972; van Dam *et al.* 2007).

We compared the vertical movements observed by GPS with those calculated from the GRACE data. Here, we used the data at 83 continuous GPS stations deployed by the International GNSS Service. All GPS data are processed by SOPAC (University of California San Diego) and available at ftp://garner.ucsd.edu/pub/timeseries/. In each GPS time-series, we eliminated the outliers deviating by more than three-sigma formal errors from models (composed of seasonal, linear and quadratic components). One-sigma formal errors are inferred *a posteriori*
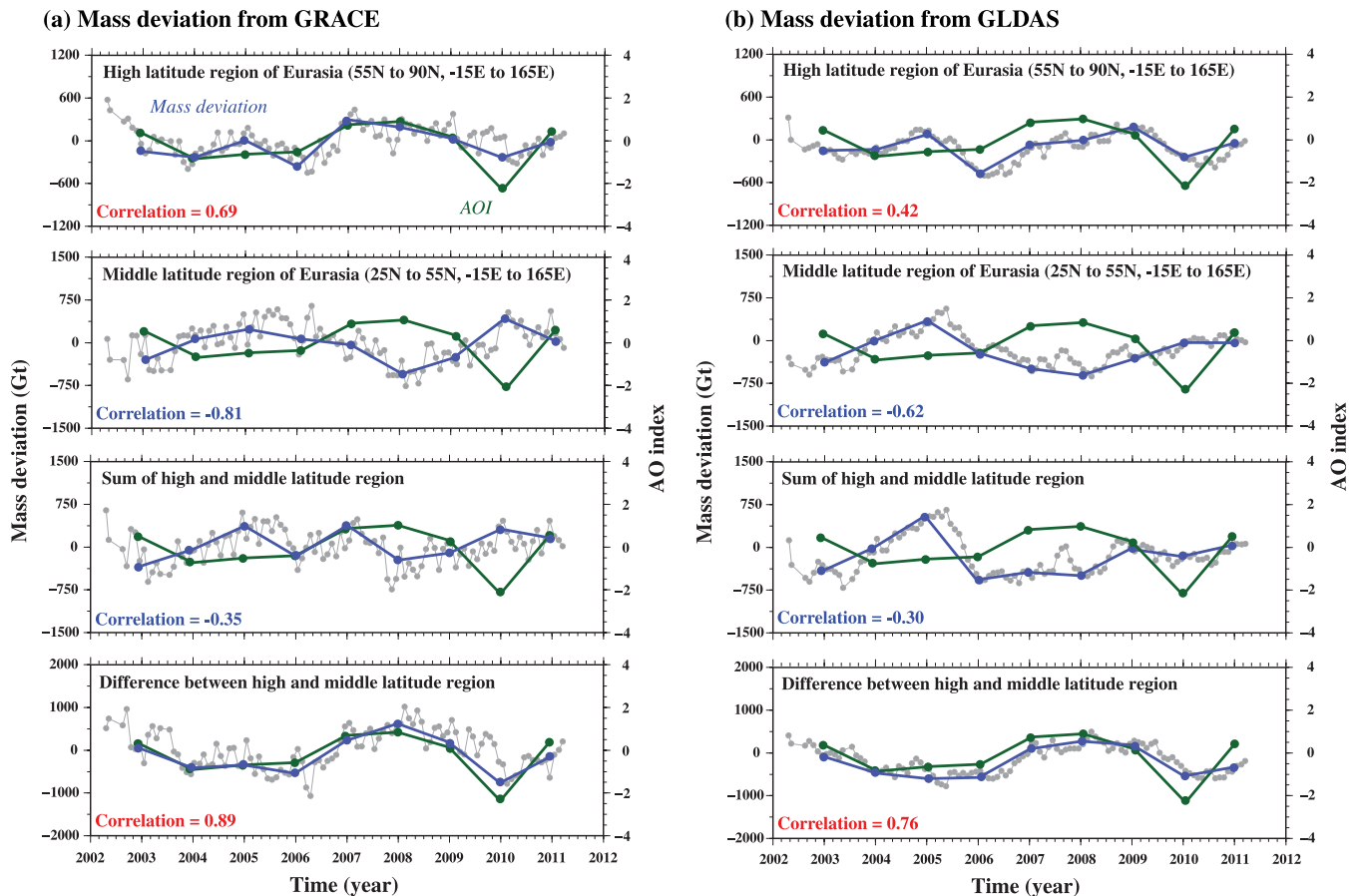
(a) Mass deviation from GRACE

(b) Mass deviation from GLDAS

Figure 6. From top to bottom, time-series of mass deviation in high latitude region (55N-90N), middle latitude region (25N-55N), the sum of the two regions, the difference between the two regions, calculated from (a) the GRACE data and (b) the GLDAS models. Grey dots are monthly values of mass deviations. Blue and green curves are the three-month (JFM) averages of mass deviations and AOI. The correlation coefficients between wintertime mass deviations and AOI are shown in the lower left corners. Red and blue characters show positive and negative correlations, respectively.

by bringing the chi-square of the post-fit residuals to unity. Deformations because of atmospheric loads are also removed from the GPS data using the European Centre for Medium-Range Weather Forecasts atmospheric model. In the same manner as GRACE and GLDAS analysis, we computed the average residuals over the three winter months (JFM) of the GPS vertical coordinates to infer AO signatures.

Vertical movement induced by AO was found to be up to $\sim$5 mm, large enough to be detected by GPS. The correlation coefficients between wintertime vertical position residuals at GPS stations and AOI are shown in Fig. 7. Positive correlations mean that the surface is uplifted/depressed by positive/negative AO, and negative correlations imply the opposite. Positive correlations are mostly found in middle latitude stations of Eurasia, North America and southern Greenland. On the other hands, negative correlations are dominant in high latitude stations of Eurasia, North America and northern Greenland. This result is just consistent with the correlation pattern between wintertime EWD and AOI (Fig. 5). We can summarize the relationship among GPS, EWD and AO as follows. In the high latitude region and northern Greenland, GPS stations are displaced downward/upward by positive/negative EWD brought about by positive/negative AO. In the middle latitude region and southern Greenland, GPS stations move upward/downward by negative/positive EWD caused by positive/negative AO.

Fig. 7 also shows the time-series of vertical movements at six continuous GPS stations, (a) Vancouver (49.3N, 235.9E), Canada,

(b) Washington, D.C. (38.9N, 282.9E), United States, (c) Cornwallis Island (82.5N, 297.7E), near Northern Greenland, (d) Qaqortoq (60.7N, 314.0E), Southern Greenland, (e) Norilsk (69.4N, 88.4E), near the West Siberian Plain and (f) Selezaschita (43.2N, 77.0E), near the Tien-Shan Mountain Ranges. We confirmed that the behaviours of GPS, GRACE and AOI are in good agreement. The correlation coefficients in the NH winters were (a) -0.59, (b) $+0.78$, (c) -0.56, (d) $+0.72$, (e) -0.81, (f) $+0.63$ for GPS-AOI, and (a) -0.45, (b) $+0.93$, (c) -0.67, (d) $+0.74$, (e) -0.95, (f) $+0.71$ for GRACE-AOI, respectively.

3.5 Polar motion excitation by AO

Large hydrological mass redistribution by AO would also excite the Earth's polar motion (Chao 1988). Its X (towards the Greenwich Meridian) and Y (towards 90E) components can be inferred from ΔC_{21} and ΔS_{21}, respectively, the changes in the degree-2 tesseral components of the gravity changes observed by GRACE (e.g. Chen & Wilson 2008).

The mass redistribution by AO occurs mainly in Eurasia, and it accounts for $\tilde{8}0$ per cent of the total amount of mass changes in the NH winters. Hence, AO would excite the polar motion mainly through mass changes in Eurasia. Here we compare (1) the polar motion excitations in the X and Y axes observed by space geodetic techniques, such as the Very-Long-Baseline
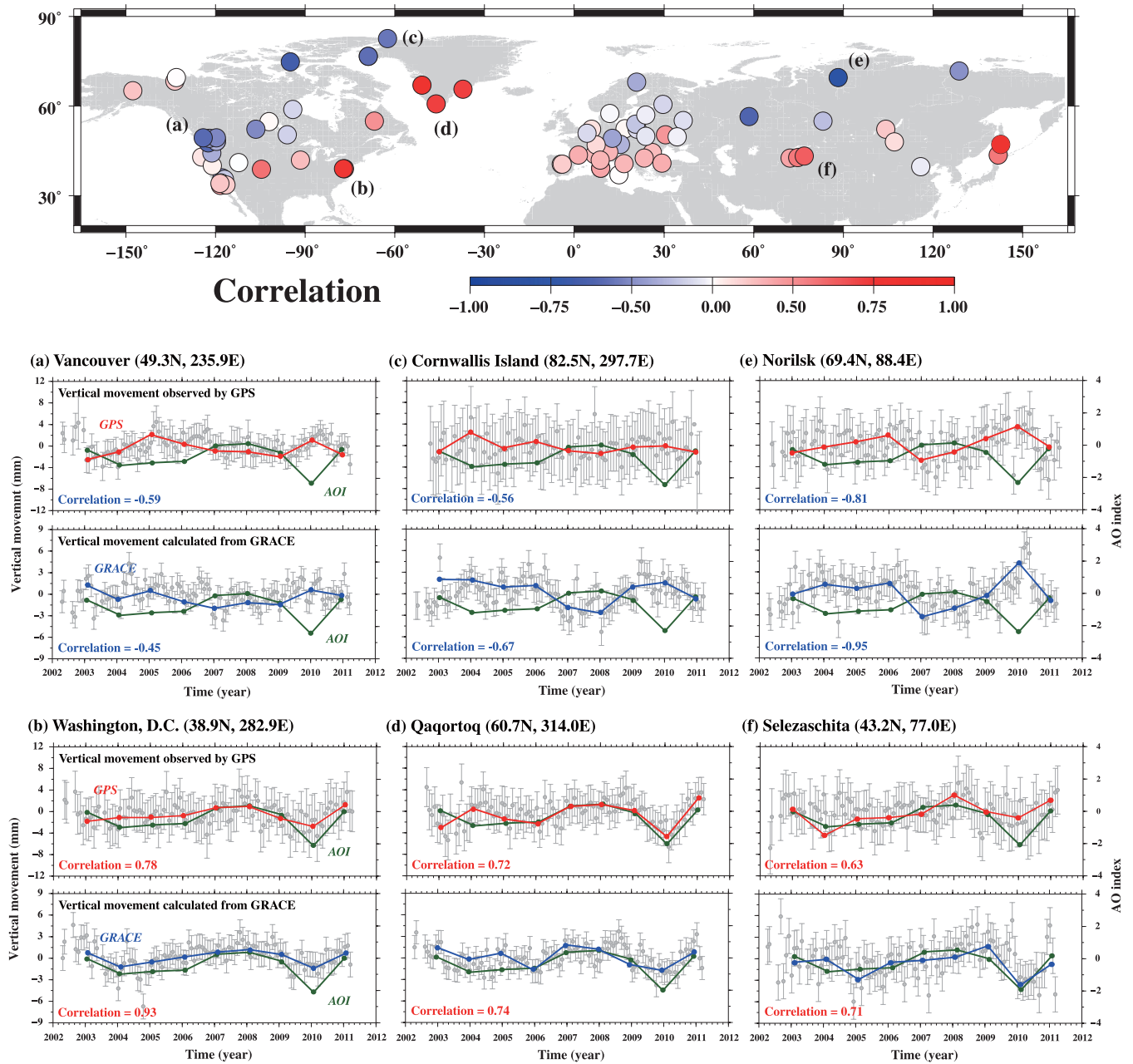
Figure 7. Upper map shows distribution of the correlation coefficients between vertical movement and AO indices at each continuous GPS station. Red dots mean positive correlation and blue dots mean negative correlation. Lower graphs show time-series of vertical movements at (a) Vancouver (49.3N, 235.9E), Canada, (b) Washington, D.C. (38.9N, 282.9E), United States, (c) Cornwallis Island (82.5N, 297.7E), near Northern Greenland, (d) Qaqortoq (60.7N, 314.0E), Southern Greenland, (e) Norilsk (69.4N, 88.4E), near the West Siberian Plain and (f) Selezaschita (43.2N, 77.0E), near the Tien-Shan Mountain Ranges, observed by GPS (upper) and inferred from the GRACE data (lower). Grey dots are monthly values of vertical movement after removing seasonal, linear, and quadratic components. The atmospheric loading contributions are removed from the GPS data using the ECMWF atmospheric model. Blue and red curves are the three-month (JFM) averages of the vertical movements measured by GPS and inferred from GRACE, respectively. Green curves show AOI. Error bars in GPS are one *SD* and those in GRACE are one-sigma formal errors inferred *a posteriori* by bringing the chi-square of the post-fit residuals to unity.

Interferometry (VLBI), with (2) NH wintertime mass changes inferred from the observed time-variable gravity changes in Eurasia. The polar motion excitations (1) are obtained from the Observatoire de Paris (OP) (http://hpiers.obspm.fr/eop-pc) after correcting for geophysical fluid (atmosphere and ocean, both mass and velocity terms) contributions using geophysical models (these corrections are also available from OP). Those from GRACE (2) are calculated by integrating the mass changes over the high and middle latitude regions in Eurasia (25N to 90N, −15E to 165E) and

by converting them to the components ΔC_{21} and ΔS_{21} (i.e. we did not use these coefficients available as the direct outputs of GRACE level-2 data but isolated the Eurasian contribution in these coefficients).

We show the results in Figs 8(a) and (b). The observed X and Y excitation (1) showed good agreement with the Eurasian mass changes inferred from GRACE (2), that is +0.51 for X and +0.58 for Y. This suggests that the NH wintertime polar motions are largely excited by mass changes there. The polar motion excitation
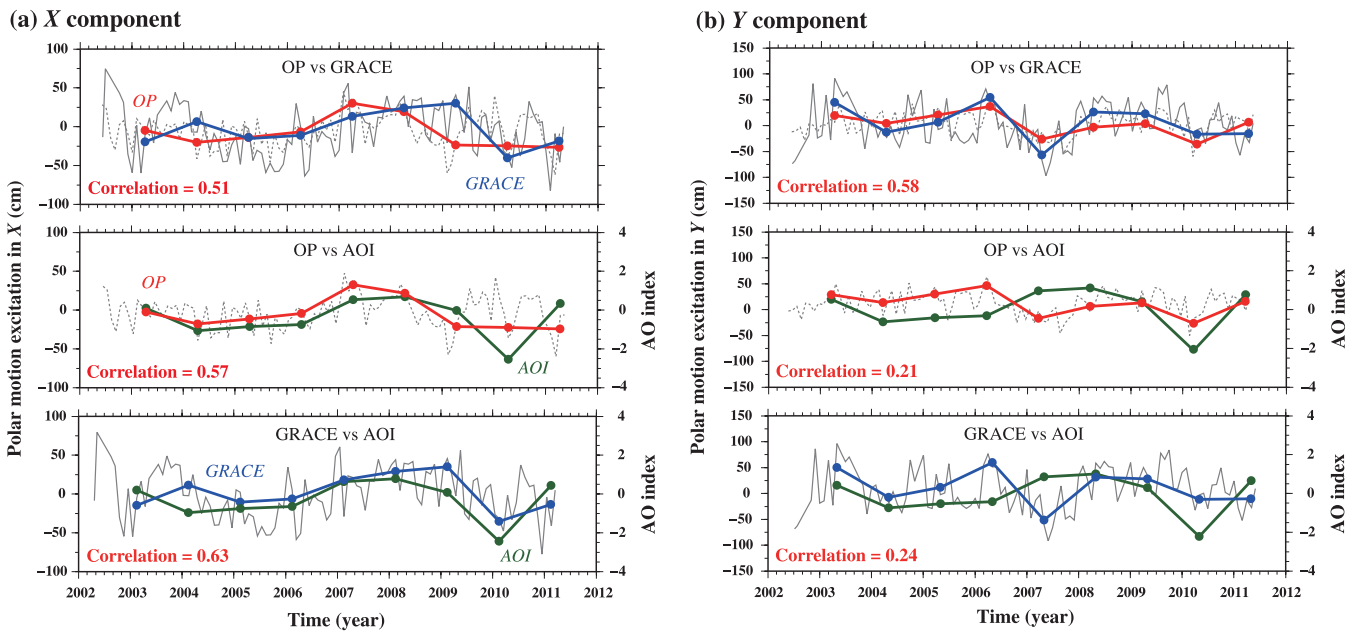
(a) *X* component

(b) *Y* component

Figure 8. Time-series of the polar motion excitation in (a) *X* (0E) and (b) *Y* direction (90E) estimated from the observations of Earth rotation parameters from the Observatoire de Paris (OP) and calculated from mass changes over Eurasia from the GRACE gravimetry. The polar motion observations are based on space geodetic techniques such as the Very-Long-Baseline Interferometry (VLBI). The upper, middle and lower panels compare pairs of OP-GRACE, OP-AOI and GRACE- AOI, respectively. Dashed and solid curves in grey are monthly values of the polar motion excitation from OP (daily values are averaged to monthly values) and GRACE, respectively. Seasonal, linear and quadratic components of these two time-series are removed using least-squares method. Polar motion excitation data are corrected for the geophysical fluid contributions (atmosphere and ocean) available from OP. Blue and red curves are the three months (JFM) averages of the polar motion excitations and GRACE, respectively. Green curves show those of AOI.

in the *X*-axis from OP (1) and GRACE (2) showed strong positive correlation (+0.57 and +0.63) with AOI whereas those in the *Y*-axis showed much weaker correlation (+0.21 and +0.24).

This suggests that positive AO moves the excitation pole towards ~0E (negative AO reverses the situation). This may sound strange considering that the centre of the Eurasian continent lies in the *Y* direction. As seen in Fig. 7(a), AO exchanges the terrestrial water mass between middle and high latitude regions in Eurasia in response to its polarity, and their centres of mass lie around (40N, 40E) and (60N, 75E), respectively. If a point mass of 1000 Gt moved from (40N, 40E) to (60N, 75E), the excitation pole would move ~101 cm towards *X* and ~36 cm towards *Y*. The reverse movement would let the excitation pole move back to the original position. Thus, AO excites the polar motion more in the *X* direction than in *Y* through the terrestrial water mass redistribution in Eurasia. As a consequence, the polar motion excitation along the *X*-axis is more strongly correlated with AOI.

4 DISCUSSION

4.1 Contributions of various climatic modes to mass changes in NH winters

There are climatic modes other than AO that may influence continental water mass changes in NH winters. One such mode is the ENSO, an episodic change in sea surface temperature in the equatorial eastern Pacific Ocean for a half year or more. An ENSO episode causes climate changes such as precipitation anomaly not only in the equatorial Pacific area, but also in remote areas by teleconnection (e.g. Ropelewski & Halpert 1987). Another prominent mode in the NH winter would be the Pacific-North American (PNA) pat-

tern (Wallace & Gutzler 1981). PNA is strongly linked to climate variations in the Pacific Ocean and North America and large-scale atmospheric circulation across North America. The intensity and polarity of these modes are expressed with the Southern Oscillation Index (SOI) and the Pacific-North American Index (PNAI) for ENSO and PNA, respectively.

Here we compare contributions of AO, ENSO and PNA, to wintertime EWD in NH by performing the EOF analysis following the method of Quadrelli *et al.* (2001). EOF analysis, also known as the Principal Component Analysis, enables us to extract principal changing mode in time-series of the data set and to separate spatial variability (spatial function) from temporal variability (temporal function). EOFs can be derived as eigenvectors of the covariance matrix of the data set. We performed the EOF analysis of wintertime EWD time-series from GRACE for the entire NH and three specific regions, that is Eurasia (25N-90N, −15E-165E), North America (25N-75N, 195E-300E) and Greenland (55N-90N, 285E-345E).

The spatial function of the first leading mode for NH (Fig. 9a) shows the polarity reversals around 55N in Eurasia and North America, and around 75N in Greenland. Contribution of this first mode accounts for ~30 per cent of all modes (Fig. 9c). Such spatial patterns are in good agreement with those of the correlation coefficients between wintertime EWD and AOI (Fig. 5). Similarly, the temporal functions are highly correlated (+0.90) with AOI (Fig. 9b). These results suggest that the first leading mode of GRACE, after removing seasonal, linear and quadratic components, corresponds to the precipitation anomalies by AO. As for other climate modes, the correlations are +0.45 for SOI and −0.56 for PNAI, respectively, which is much smaller than AOI. The ENSO signature could be found as the third mode (the correlation coefficient of −0.68 between wintertime SOI and the temporal function).
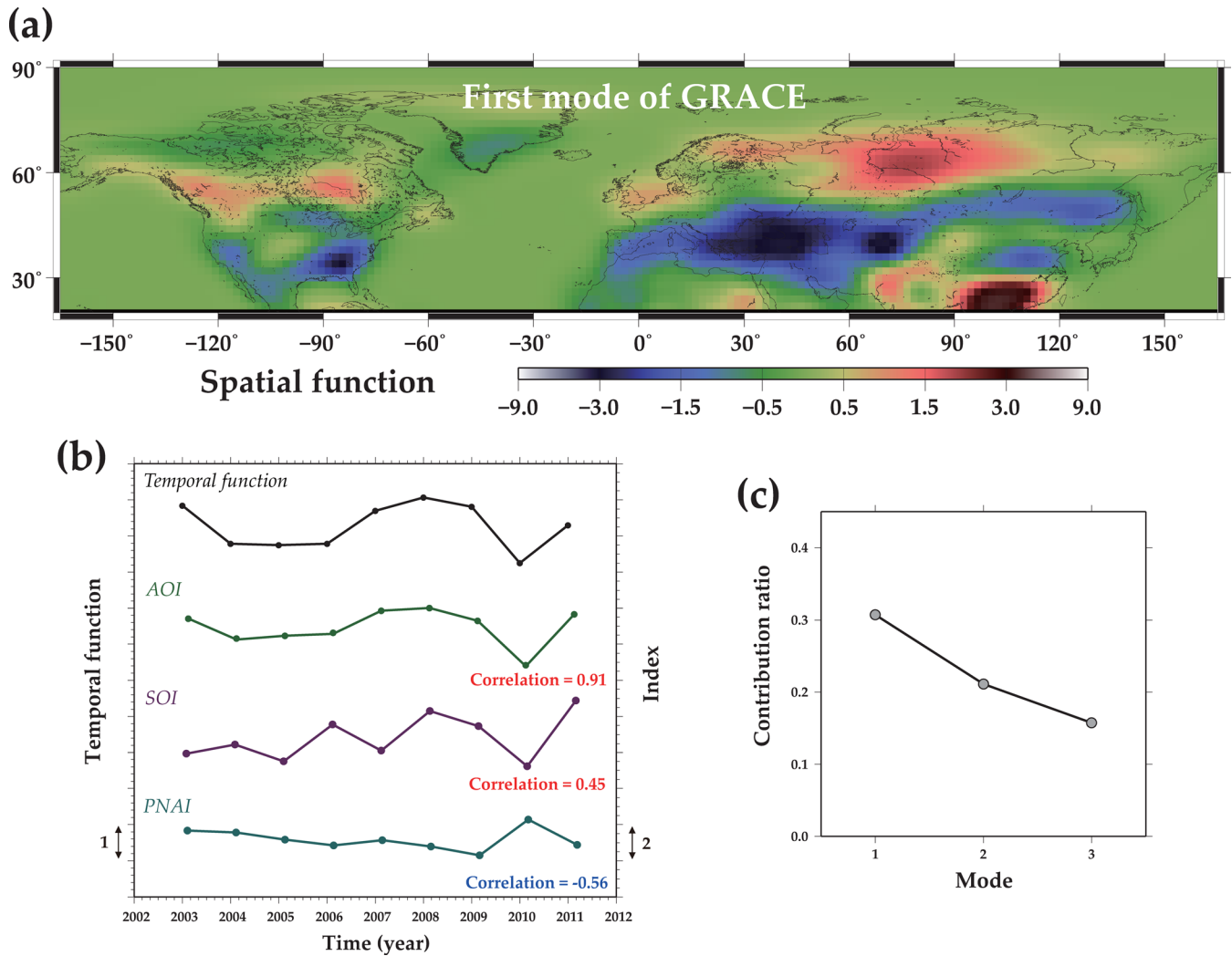
(a)

Figure 9. (a) Spatial and (b) temporal functions of the first leading mode derived by the EOF analysis of wintertime mass changes from GRACE after removal of seasonal, linear and quadratic components. Weight factor of the cosine of latitude was applied for the GRACE data. Black, green, purple and light blue curves are the three-month (JFM) averages of the time functions, AOI, SOI and PNAI, respectively. SOI is obtained from http://www.cpc.ncep.noaa.gov/data/indices/soi, and PNAI is obtained from http://www.cpc.ncep.noaa.gov/products/precip/CWlink/pna/pna_index.html. Strong positive correlation can be found between the time functions and AOI. (c) Contributions of the largest 3 modes. The first mode contributes by ∼30 per cent.

Fig. 10 shows the spatial and temporal functions of the first leading mode of regional GRACE data of Eurasia (a), North America (b) and Greenland (c). The results of Eurasia and Greenland agree well with those of the entire NH, as seen by the high correlation (+0.86 and +0.84, respectively) with AOI. North America, however, seems to behave somewhat differently from them; terrestrial water storage there is more influenced by ENSO (correlation: +0.80) than AO (correlation: +0.53). The spatial function also resembles to the precipitation anomaly pattern of ENSO (e.g. Ropelewski & Halpert 1987). After all, AO is the largest contributor to the wintertime terrestrial water storages of the entire NH, but ENSO also plays a dominant role regionally in North America.

4.2 Influence of temperature anomaly by AO to terrestrial water storage

AO influences surface air temperature (SAT) over NH. Positive AO tends to increase/decrease SAT north/south of ∼45N in Eurasia, decrease/increase SAT north/south of ∼45N in North America and
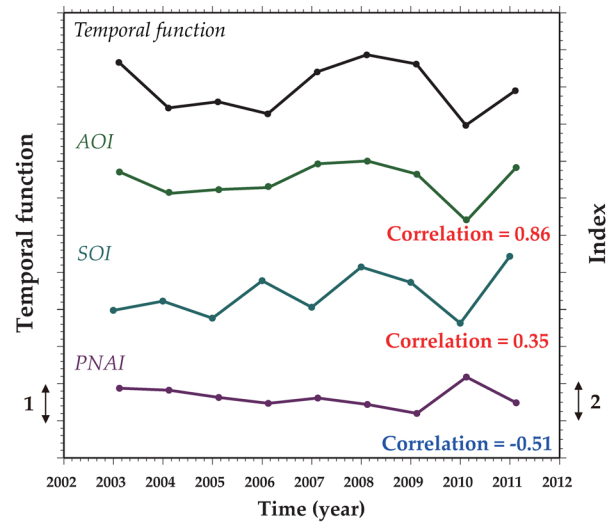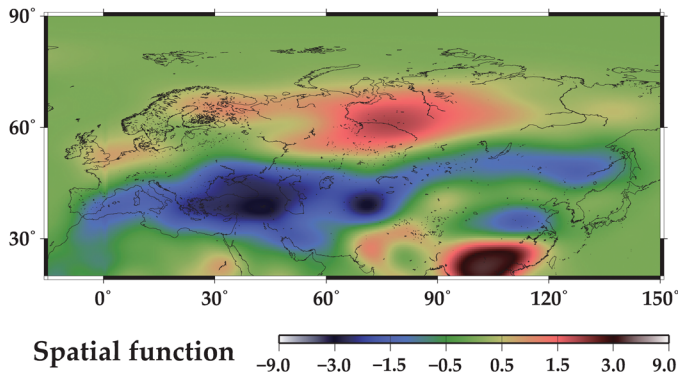
decrease SAT in Greenland (Thompson & Wallace 1998). Negative AO reverses the situation. In the 2010 winter, a year of the record-breaking strong negative AO, SAT anomaly attains up to ∼2.5 °C in each continent (Cohen *et al.* 2010). Such anomalous SAT would influence terrestrial water storage through evaporation, snow melting and run-off (increase/decrease of SAT enhances/reduces them).

The balance between precipitation-driven mass change and temperature-driven mass changes (evapo-transpiration, snow melting and run-off) can be evaluated through the framework of GLDAS model. GLDAS suggests that total water budget has much more similar distribution in space and sense to precipitation than evapo-transpiration, snow melting and run-off. Off course, temperature anomaly by AO must contribute to the changes in terrestrial water storage. However, in this case, temperature appears to play a lesser role in terrestrial water storage than precipitation.
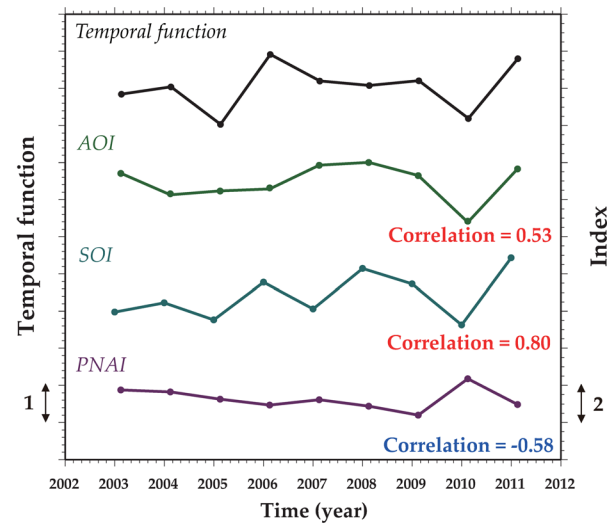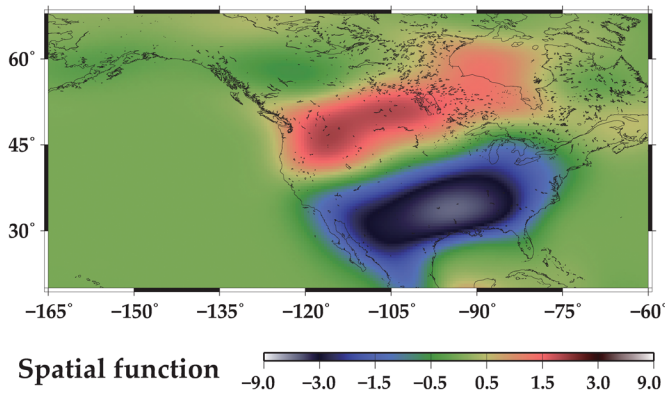
5 CONCLUSION

We have analysed 9 yr of time-variable gravity data by the GRACE satellites, and the GLDAS land hydrological models to investigate
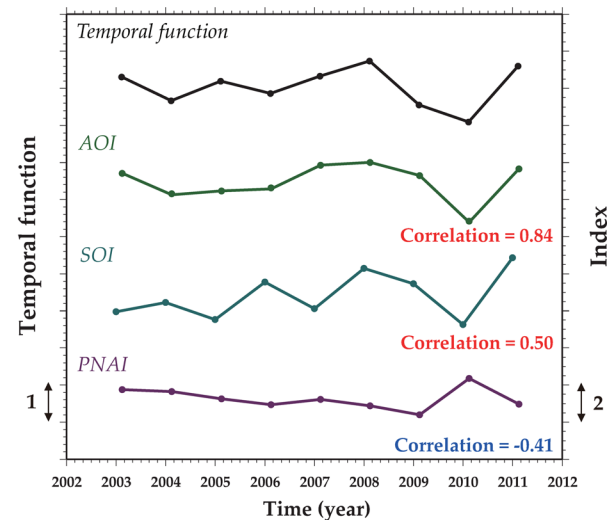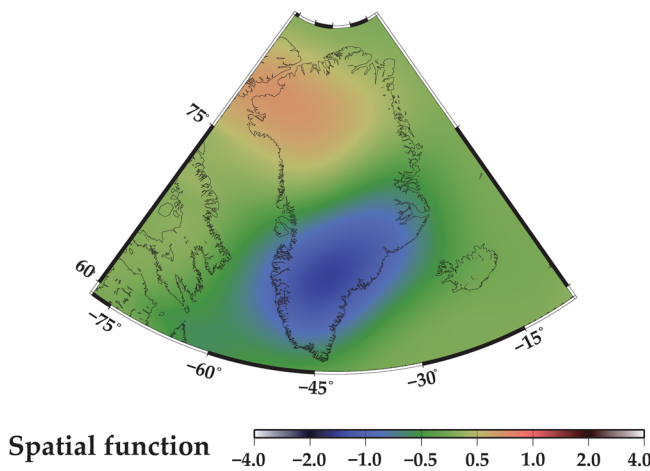
Figure 10. Spatial (left) and temporal (right) functions of the first leading mode derived by the EOF analysis of wintertime mass deviations from GRACE for the three regions, namely (a) Eurasia, (b) North America and (c) Greenland. Black, green, purple and light blue curves are the three-month (JFM) averages of the indices AOI, SOI and PNAI, respectively. Contribution of the first mode was 39 per cent for Eurasia, 47 per cent for America and 44 per cent for Greenland. Time functions in Eurasia and Greenland show high correlations with AOI whereas that in North America resembles more to SOI.

signatures of precipitation anomalies in NH winters caused by AO. Our study is summarized as follows.

(1) Positive and negative AO are considered to enhance wintertime precipitations in the high and middle latitude regions in NH, respectively, and such mass redistributions can be seen in the GRACE data.

(2) The distribution of the correlation coefficients between precipitation anomalies and AOI shows characteristic patterns; that is boundary of the positive and negative correlations lie along the latitude of ~55N in Eurasia and North America, and along ~75N in Greenland.

(3) AO moves the center of precipitation depending on its polarity. AO could move mass as large as ~1000 Gt over the distance of ~2000 km like a see-saw between these two regions in response to its polarity.

(4) The mass movements by AO are also observed as the surface deformation using GPS. The surface deformation shows similar correlation pattern with AOI to the GRACE data.

(5) The mass movements by AO excite the Earth's polar motion above the detection level of space geodetic techniques, such as VLBI. The excitation pole was found to move mainly along the X-axis.

(6) EOF analyses showed that the AO signature is the leading mode of the GRACE gravity data after removing seasonal, linear and quadratic components.

(7) Other climatic modes, ENSO and PNA, also influence wintertime terrestrial water storages, but their contributions to the whole NH are smaller than AO.

This study is the first attempt to explore the AO-driven mass redistribution signatures in the time-variable gravity field observed by GRACE. The implication of this research is threefold. At first, GRACE is a new tool, and we need to know how a known climatological phenomenon appear in GRACE data to identify unknown signals (such as co- and post-seismic gravity changes). Second, GRACE is the only tool to directly measure global-scale mass redistributions. It would enable us to study mass balances in polar and high mountain regions where *in situ* observations are limited or unavailable. In fact, this study revealed characteristic links between AO and mass changes in Greenland and northwestern Asian High Mountains. As the third point, GRACE enables us to see precipitation anomalies through a filter of terrestrial water storage. Precipitation anomaly and the water storage anomaly are not equivalent; the latter reflects not only precipitation but also factors such as water storage capacity, run-off time constants, land-ocean distribution, etc. Scrutiny of their differences will enable us to further understand the link between changes in climate and water resources.

ACKNOWLEDGMENTS

REFERENCES

Ambaum, M.H.P., Hoskins, B.J. & Stephenson, D.B., 2001. Arctic Oscillation or North Atlantic Oscillation?, *J. Clim.,* **14,** 3495–3507, doi:10.1175/1520-0442(2001)014<3495:AOONAO>2.0.CO;2.

Ball, S., 2011. Exceptional rainfall in Gibraltar during winter 2009/2010, *Weather,* **66**(1), 22–25, doi:10.1002/wea.733.

Chambers, D.P., Wahr, J. & Nerem, R.S., 2004. Preliminary observations of global ocean mass variations with GRACE, *Geophys. Res. Lett.,* **31,** L13310, doi:10.1029/2004GL020461.

Chao, B.F., 1988. Excitation of the earth's polar motion due to mass variations in major hydrological reservoirs, *J. geophys. Res.,* **93**(B11), P13811–P13819, doi:10.1029/JB093iB11p13811.

Chao, B.F., 2005. On inversion for mass distribution from global (time-variable) gravity field, *J. Geodyn.,* **39,** 223–230, doi:10.1016/j.jog.2004.11.001.

Chen, J.L., Tapley, B.D. & Wilson, C.R., 2006. Alaskan mountain Glacial melting observed by Satellite gravimetry, *Earth planet. Sci. Lett.,* **248,** 368–378, doi:10.1016/j.epsl.2006.05.039.

Chen, J.L. & Wilson, C.R., 2008. Low degree gravity changes from GRACE, Earth rotation, geophysical models, and satellite laser ranging, *J. geophys. Res.,* **113,** B06402, doi:10.1029/2007JB005397.

Cheng, M. & Tapley, B.D., 2004. Variations in the Earth's oblateness during the past 28 years, *J. geophys. Res.,* **109,** B09402, doi:10.1029/2004JB003028.

Cohen, J., Foster, J., Barlow, M., Saito, K. & Jones, J., 2010. Winter 2009–2010: a case study of an extreme Arctic Oscillation event, *Geophys. Res. Lett.,* **37,** L17707, doi:10.1029/2010GL044256.

Farrell, W.E., 1972. Deformation of the Earth by surface loads, *Rev. Geophys. Space Phys.,* **10**(3), 761–797.

Fenoglio-Marc, L., Kusche, J. & Becker, M., 2006. Mass variation in the Mediterranean Sea from GRACE and its validation by altimetry, steric and hydrologic fields, *Geophys. Res. Lett.,* **33,** L19606, doi:10.1029/2006GL026851.

Frappart, F., Ramillien, G., Biancamaria, S., Mognard, N.M. & Cazenave, A., 2006. Evolution of high-latitude snow mass derived from the GRACE gravimetry mission (2002–2004), *Geophys. Res. Lett.,* **33,** L02501, doi:10.1029/2005GL024778.

Gardner, A.S. *et al*., 2011. Sharply increased mass loss from glaciers and ice caps in the Canadian Arctic Archipelago, *Nature,* **473,** 357–360, doi:10.1038/nature10089.

Han, S.C., Shum, C.K., Bevis, M., Ji, C. & Kuo, C.-Y., 2006. Crustal dilatation observed by GRACE after the 2004 Sumatra-Andaman earthquake, *Science,* **313,** 658–666, doi:10.1126/science.1128661.

Hurrell, J.M., 1995. Decadal trends in the North Atlantic Oscillation: regional temperature and precipitation, *Science,* **269,** 676–679, doi:10.1126/science.269.5224.676.

Hurrell, J.M., Kushnir, Y., Ottersen, G. & Visbeck, M., 2003. An overview of the North Atlantic Oscillation, in *The North Atlantic Oscillation: Climatic Significance and Environmental Impact,* Geophys. Monogr. Ser. Vol. 134, pp. 1–35, eds Hurrell, J.M., Kushnir, Y., Ottersen, G. & Visbeck, M., American Geophysical Union, Washington, D.C.

L'Heureux, M. *et al*., 2010. Unusual extremes in the negative phase of the Arctic Oscillation during 2009, *Geophys. Res. Lett.,* **37,** L10704, doi:10.1029/2010GL043338.

Matsuo, K. & Heki, K., 2010. Time-variable ice loss in Asian high mountains from satellite gravimetry, *Earth planet. Sci. Lett.,* **290,** 30–36, doi:10.1016/j.epsl.2009.11.053.

Matsuo, K. & Heki, K., 2011. Coseismic gravity changes of the 2011 Tohoku-Oki Earthquake from satellite gravimetry, *Geophys. Res. Lett.,* **38,** L00G12, doi:10.1029/2011GL049018.

Morishita, Y. & Heki, K., 2008. Characteristic precipitation patterns of El Niño/La Niña in time-variable gravity fields by GRACE, *Earth planet. Sci. Lett.,* **272,** 677–682, doi:10.1016/j.epsl.2008.06.003.

Ogawa, R., Chao, B.F. & Heki, K., 2011. Acceleration signal in GRACE time-variable gravity in relation to interannual hydrological changes, *Geophys. J. Int.,* **184,** 673–679, doi:10.1111/j:1365-246X.2010.04843.x.

Quadrelli, R., Pavan, V. & Molteni, F., 2001. Wintertime variability of Mediterranean precipitation and its link with large-scale circulation anomalies, *Clim. Dyn.,* **17,** 457–466.

Rodell, M. *et al*., 2004. The Global Land Data Assimilation System, *Bull. Am. Meteorol. Soc.,* **85,** 381–394.

Ropelewski, C.F. & Halpert, M.S., 1987. Global and regional scale precipitation patterns associated with the El Niño/southern oscillation, *Mon. Weather Rev.,* **115,** 1606–1626.

Schmidt, R., Petrovic, S., Guntner, A., Barthelmes, F., Wunsch, J. & Kusche, J., 2008. Periodic components of water storage changes from GRACE and global hydrology models, *J. geophys. Res.,* **113,** B08419, doi:10.1029/2007JB005363.

Seager, R., Kushnir, Y., Nakamura, J., Ting, M. & Naik, N., 2010. Northern hemisphere winter snow anomalies: ENSO, NAO and the winter of 2009/10, *Geophys. Res. Lett.,* **37,** L14703, doi:10.1029/2010GL043830.

Steffen, H., Gitlein, O., Denker, H., Müller, J. & Timmen, L., 2009. Present rate of uplift in Fennoscandia from GRACE and absolute gravimetry, *Tectonophysics,* **474,** 69–77, doi:10.1016/j.tecto.2009.01.012474.

Syed, T.H., Famiglietti, J.S., Rodell, M., Chen, J. & Wilson, C.R., 2008. Analysis of terrestrial water storage changes from GRACE and GLDAS, *Water Resour. Res.,* **44,** W02433, doi:10.1029/2006WR005779.

Swenson, S. & Wahr, J., 2006. Post-processing removal of correlated errors in GRACE data, *Geophys. Res. Lett.,* **33,** L08402, doi:10.1029/2005GL025285.

Swenson, S., Chambers, D. & Wahr, J., 2008. Estimating geocenter variations from a combination of GRACE and ocean model output, *J. geophys. Res.,* **113,** B08410, doi:10.1029/2007JB005338.

Tamisiea, M.E., Leuliette, E.W., Davis, J.L. & Mitrovica, J.X., 2005. Constraining hydrological and cryospheric mass flux in southeastern Alaska using space-based gravity measurements, *Geophys. Res. Lett.,* **32,** L20501, doi:10.1029/2005GL023961.

Tamisiea, M.E., Mitrovica, J.X. & Davis, J.L., 2007. GRACE gravity data constrain ancient ice geometries and continental dynamics over Laurentia, *Science,* **316,** 881–883, doi:10.1126/science.1137157.

Tapley, B.D., Bettadpur, S., Ries, J.C., Thompson, P.F. & Watkins, M.M., 2004. GRACE measurements of mass variability in the earth system, *Science,* **305,** 503–505, doi:10.1126/science.1099192.

Thompson, D.W.J. & Wallace, J.M., 1998. The Arctic Oscillation signature in the wintertime geopotential height and temperature fields, *Geophys. Res. Lett.,* **25,** 1297–1300, doi:10.1029/98GL00950.

Thompson, D.W.J. & Wallace, J.M., 2000. Annular modes in the extratropical circulation, Part I: Month-to-Month variation, *J. Clim.,* **13,** 1000–1016, doi:10.1175/1520-0442(200)013<1000:AMITEC>2.0.CO;2.

Thompson, D.W.J. & Wallace, J.M., 2001. Regional climate impacts of the Northern Hemisphere Annular Mode and associated climate trends, *Science,* **293,** 85–89, doi:10.1126/science.1058958.

van Dam, T., Wahr, J. & Lavallée, D., 2007. A comparison of annual vertical crustal displacements from GPS and Gravity Recovery and Climate Experiment (GRACE) over Europe, *J. geophys. Res.,* **112,** B03404, doi:10.1029/2006JB004335.

Velicogna, I. & Wahr, J., 2006a. Measurements of time-variable gravity show mass loss in Antarctica, *Science,* **311**(5768), 1754–1756, doi:10.1126/science.1123785.

Velicogna, I. & Wahr J., 2006b. Acceleration of Greenland ice mass loss in spring 2004, *Nature,* **443,** 329–331, doi:10.1038/nature05168.

Wahr, J., Molenaar, M. & Bryan, F., 1998. Time variability of the Earth's gravity field: hydrological and oceanic effects and their possible detection using GRACE, *J. geophys. Res.,* **103,** 30 205–30 229, doi:10.1029/98JB02844.

Walker, G.T. & Bliss, E.W., 1932. World weather V, *Mem. R. Meteorol. Soc.,* **4,** 53–83.

Wallace, J.M., 2000. North Atlantic Oscillation/annular mode: two paradigms-one phenomenon, *Q. J. R. Meteorol. Soc.,* **126,** 791–805.

Wallace, J.M. & Gutzler, D.S., 1981. Teleconnection in the geopotential height field during the Northern Hemisphere winter, *Mon. Wea. Rev.,* **109,** 784–812.

Wang, C., Liu, H. & Lee, S., 2010. The record-breaking cold temperatures during the winter of 2009/2010 in the Northern Hemisphere, *Atmos. Sci. Lett.,* **11,** 161–168, doi:10.1002/asl.278.

Zhang, Z.Z., Chao, B.F., Lu, Y. & Hsu, H.-T., 2009. An effective filtering for GRACE time-variable gravity: fan filter, *Geophys. Res. Lett.,* **36,** L17311, doi:10.1029/2009GL039459.